Biochimica et Biophysica Acta 1848 (2015) 2394–2405

Contents lists available at ScienceDirect

Biochimica et Biophysica Acta

journal homepage: www.elsevier.com/locate/bbamem

The structure and behavior of the NA-CATH antimicrobial peptide with liposomes

Haijuan Du [1], Robin L. Samuel [1], Michael A. Massiah *, Susan D. Gillmor *

Department of Chemistry, George Washington University, Washington DC 20052, United States

ARTICLE INFO

Article history:
Received 10 April 2015
Received in revised form 1 July 2015
Accepted 16 July 2015
Available online 21 July 2015

Keywords:
Peptide structure
NA-CATH
NMR structure
Antibacterial
Antimicrobial
AMP
Amphipathic helix
Protein–liposome interaction
Fluorescence requenching

ABSTRACT

Naja atra cathelicidin (NA-CATH) is a 34-amino acid highly cationic peptide identified in Chinese cobras to possess potent toxicity against gram-negative and gram-positive bacteria and low toxicity against host cells. Here, we report the NMR solution structure of the full-length NA-CATH peptide and its interaction with liposomes. The structure shows a well-defined α-helix between residues Phe3 to Lys23, on which one surface is lined by the side-chains of one arginine and 11 lysine residues, while the other side is populated by hydrophobic residues. The last eleven amino acids, which are predominately aromatic and hydrophobic in nature, have no defined structure. NMR data reveal that these residues do not interact with the hydrophobic residues of the helix, indicating that the C-terminal residues have random conformations. Fluorescence requenching experiments, in which liposomes serve as a mimic of the bacterial membranes, result in fluorophore leakage that is consistent with a membrane thinning or transient pore formation mechanism. NMR titration studies of the peptide–liposome interaction reveal that the peptide is in fast exchange with the liposome, consistent with the fluorescent studies. These data indicate that full length NA-CATH possesses a helical segment and unstructured C-terminal tail that disrupts the bilayer to induce leakage and lysing.

1. Introduction

Antimicrobial peptides (AMPs) are an essential component of immune systems of living organisms, and exert a direct effect on a broad spectrum of microbes including bacteria, fungi, and viruses [1–4]. They also have a wide variety of functions within the host, including immunomodulatory and chemoattractant agents [5,6]. Several AMPs have been shown to exhibit cytotoxic activity against cancer cells and have shown promise as anticancer drugs [7]. Currently, there are more than 2500 antimicrobial peptides identified and most are often less than 100 amino acids and possess numerous cationic residues, specifically lysine and arginine [1,8]. AMPs exhibit a diverse range of amino acid sequences and structural properties. They are classified into four groups based on structural themes: linear α-helical peptides, linear extended peptides (with sequences dominated by a few types of amino acids), peptides containing loop structures, and peptides with structures constrained by intra-molecular disulfide bonds [9].

Given the wide range of attributes, structures, and sequences, AMPs also exhibit various behaviors in their antibacterial role. Translocated peptides into the bacterium lead to the disruption of cellular processes, such as syntheses of nucleic acids, proteins, and cell walls [10–13] and enzymatic activity [14] to name a few [11,15]. The most common mode of action involves the disruption membrane function and integrity [16–18]. In our system, we have reported that the cathelicidin, NA-CATH, from the *Naja atra* snake, targets the membrane both in models and in cell studies [19], leading us to investigate its structure and lysing characteristics to clarify its behavior.

Within the general membrane disruption category, two primary mechanisms are hypothesized: pore formation and disruption of membrane integrity [1,9,17,20–35]. The Shai–Matsuzaki–Huang [36–39] model suggests that the amphipathic AMPs must first interact with the membrane surface electrostatically, and then insert into the membrane to form large pores [1,3,40]. In contrast, AMPs may exert its bactericidal effect with a detergent-like "carpet mechanism" [37], disrupting the structural properties of the membrane and resulting in curvature strain, membrane thinning, short lived defects, transient pores and even complete membrane dissolution [1,7,21,35,41,42]. Both mechanisms potentially lead to membrane depolarization, lipid flip-flop accompanied by AMP translocation, lipid clustering, and induced phase separation [7,43]. All of these effects are detrimental to membrane functions. In our study, we employ a combination of NMR and fluorescence requenching assays to distinguish between these two general models for NA-CATH, a highly cationic AMP.

The cathelicidin antimicrobial peptide obtained from the *Naja atra* snake, NA-CATH, displays highly potent, high efficacy behavior against gram-negative and gram-positive bacteria, and even biofilms [44] making it a promising candidate to combat resistant bacterial strains. Importantly, it exhibits minimal cytotoxic effect against host cells [45–47].

* Corresponding authors.
E-mail addresses: massiah@gwu.edu (M.A. Massiah), sdgill@gwu.edu (S.D. Gillmor).
[1] These authors have contributed equally.

http://dx.doi.org/10.1016/j.bbamem.2015.07.006
0005-2736/

NA-CATH has 34-amino acids and a net charge of +15, making it among the most cationic of AMPs [48]. Understanding NA-CATH structure and general behavior is critical in determining how the combination of charge, cooperativity and membrane interactions affects AMP lysing capabilities.

Previous studies reveal a semi-conserved 11 amino-acid (KRAKKFFKKLK-NH_2) motif, ATRA-1A, that has antimicrobial activity on its own, similar to the full length peptide [19]. This motif appears twice within the sequence, with only a few differences in the non-basic amino acids. Due to its length, ATRA-1A cannot span the membrane bilayer nor can it form a barrel-stave pore. Therefore, it is important to understand the structure and function of the full-length NA-CATH to distinguish possible differences in the activity of the parent and shortened peptide, as seen by Juba et al. [49].

Here, we describe the solution structure of the NA-CATH peptide by NMR spectroscopy and a mechanism of action based on fluorescence-requenching studies and titration studies by NMR. The peptide adopts an α-helical conformation between residues Phe3 and Lys23, while the remaining C-terminal 11-amino acids remain unstructured. Peptide–liposome binding studies show fast exchange between the peptide and membrane. The fluorescence and previous microscopy data give a consistent picture of liposome disruption via thinning or transient defects.

2. Experimental procedures

2.1. Materials

The peptides used in these studies were custom synthesized by GenScript (Piscataway, NJ). The supplier reported purity of NA-CATH was 95.0% based on high-performance liquid chromatography (HPLC) analysis and verified by mass spectrometry. The following lipids were purchased from Avanti Polar Lipids (Alabaster, AL) and used without modification: 1,2-dioleoyl-sn-glycero-3-phosphocholine (DOPC) and 1,2-dioleoyl-sn-glycero-3-phospho-(1′-rac-glycerol) (sodium salt) (DOPG). The following materials were obtained from Invitrogen (Carlsbad, CA): 8-aminonaphthalene-1,3,6-trisulfonic Acid, disodium salt (ANTS) and p-xylene-Bis-pyridinium bromide (DPX). Sephadex® G-25 Medium gel filtration medium and 2,2,2-trifluoroethanol-d_3 (TFE or d-TFE, 99.5% purity) were purchased from Sigma Aldrich (St. Louis, MO) [22]. Heavy water or deuterium oxide (D_2O, 99.8% purity) was purchased and used without modification from Acros (Fair Lawn, NJ).

2.2. NMR spectroscopy

The NMR sample was prepared by dissolving 2.0 mg of the lyophilized peptide (NA-CATH, K^1RFKKFFKKL^{10}KNSVKKRAKK^{20}FFKKPKVIGV^{30}TFPF) into 350 μL PBS buffer consisting of 90% H_2O/10% D_2O at pH 7.4 to yield a final concentration of ~1.5 mM. The sample was placed in a 5 mm Shigemi tube. NMR data were acquired on a 600 MHz Agilent NMR spectrometer equipped with a 5-mm triple-resonance z-axis gradient probe.

An initial two-dimensional (2D) ^1H–^1H NOESY spectrum of the peptide in PBS buffer was acquired with mixing times of 100,150, and 200 msec at 21 °C. Initial evaluation of the data indicated that the peptide did not have a stable structure because there were very little ^1H–^1H correlations from the NH protons. Subsequently, the peptide sample was titrated with 2,2,2-trifluoroethanol-d_3 (TFE) and the effect on the peptide was evaluated by one-dimensional ^1H NMR spectrum at each 10% increment. The 2D ^1H–^1H NMR data presented here were acquired with the peptide in 30% TFE. Previously, liposomes were titrated into the peptide sample to determine whether it would stabilize the peptide structure. However, no stable structure was observed and the titration instead caused liposome lysing.

Multiple 2D ^1H–^1H NOESY spectra were acquired with mixing times of 100,150, and 200 msec. The 2D TOCSY spectrum was acquired using a DIPSI-2 pulse train with a mixing time of 15 msec. A 2D DQF-COSY spectrum was acquired. The NMR data were processed by NMRpipe [50] and analyzed with SPARKY [51] software packages.

For the structure calculation, restraints were based on NOEs observed from the NOESY spectrum acquired with 100 msec mixing time. The distance restraints used for the structure calculations were grouped into three categories of 1.8–2.8 Å, 1.8–3.3 Å, and 1.8–5.0 Å corresponding to NOE intensities of strong, medium, and weak, respectively. Restraints based on NOEs to methyl and ambiguous germinal methylene protons were assigned an additional 1.0 and 0.5 Å, respectively. For restraints involving NOEs for the aromatic side-chain protons, 2.3 Å was added to account for the pseudo-atom position for the δ- and ε-protons.

A total of 399 NOE-derived restraints were used in the structure calculations. All atoms of the peptide were included in the calculations. Structures were computed using CYANA 2.1 [52] on an iMac Macintosh computer operating with OSX 10.7. From a total of 30 randomly calculated structures, 10 were selected based on low target function values of less than one and low RMSD values. Target function values, as output by CYANA, reflect energetic influences due to violations for NOE, bond length, VdW, and angles for the calculated structure. The low target function values means that there were no violations beyond what is accepted for a well-defined structure by NMR spectroscopy. A total of 20,000 steps for torsion-angle simulated annealing were employed.

2.3. Liposome preparation

Large unilameller vesicles (LUV's, ~100 nm) were used to probe the mechanism of interaction between the NA-CATH peptide and lipid vesicles. Liposomes are historically effective to employ as a membrane mimic [53–63] and to probe protein–lipid interactions [42,54,55,58–63]. Regular liposomes, needed for the peptide–liposome interaction studies by ^1H NMR, and fluorophore loaded liposomes, used in the fluorescence requenching experiment were prepared as follows. Lipids dissolved in chloroform were mixed together in a ratio of 80% zwitterionic 1,2-dioleoyl-sn-glycero-3-phosphocholine (DOPC) to 20% anionic 1,2-dioleoyl-sn-glycero-3-phospho-(1′-rac-glycerol) (sodium salt) (DOPG) and dried under nitrogen and under vacuum for 2 h. The vesicles were hydrated in PBS buffer (for NMR) or 10 mM HEPES/70 mM KCl buffer (for fluorescence assays) at pH 7. Loaded liposomes for fluorescence studies also contained the dye quencher pair 8-Aminonaphthalene-1,3,6-trisulfonic acid, disodium salt and p-xylene-Bis-pyridinium bromide (ANTS/DPX) at 10 mM and 15 mM respectively. The freeze/thaw method was employed to ensure adequate encapsulation of the dye and quencher. Briefly, the vesicles were allowed to swell for 5 min before being vortexed for 30 s. The vesicles were heated to 45 °C before undergoing five freeze/thaw cycles utilizing a dry ice/ethanol bath for 3 min, followed by a 45 °C water bath for 5 min. Excess dye and quencher molecules outside the loaded vesicles were removed by gel filtration using Sephadex G-25. This method produced a vesicle population of 90% LUVs (50–1000 nm) and 10% SUVs (less than 20 nm) as measured using Dynamic Light Scattering (Wyatt Technologies, Santa Barbara, CA). Studies conducted on samples of 100% SUVs do not exhibit any leakage (data not shown), therefore the presence of a small population of SUVs does not affect the leakage data. Concentration of the loaded vesicle was determined with a phosphate assay described elsewhere [64].

2.4. Peptide–liposome interaction by NMR spectroscopy

To test whether the α-helical peptide interacts with liposomes, we titrated liposomes (80:20 DOPC:DOPG) into ~1.6 mM peptide in PBS buffer with 30% TFE. The liposome was added in ~0.4 mM increments, from a 30 mM stock, and interaction with the peptide was monitored by chemical shift changes in the peptide ^1H signals. We also performed the liposome titration with peptide (0.25 mM) in PBS buffer without TFE.

2.5. Fluorescence requenching experiments

Fluorescence requenching studies, developed by Ladokhin et al. [65] and used by others [21,22,29,35,42] have been performed to identify the leakage mechanism of action. For a detailed summary of the technique, see Supplemental Figs. S1–S5. Briefly, liposomes are loaded with ANTS (fluorescent dye) and DPX (quencher). When the peptide interacts with the vesicles, leakage occurs, resulting in the separation of ANTS and DPX and an increase in fluorescence signal (Supplemental Fig. S1). If the quenching inside the vesicles (Q_{in}) changes due to a greater degree of leakage (f_{out}) of the dye, then the release mechanism is considered graded or gradual and Q_{in} vs. f_{out} will have the following relationship:

$$Q_{in} = \left[\left(1 + K_d * [DPX]_0 * (1-f_{out})^{\alpha}\right) * \left(1 + K_a * [DPX]_0 * (1-f_{out})^{\alpha}\right)\right]^{-1}. \quad (1)$$

In the equation, $K_{d\ [DPX]}$ is the dynamic quenching constant (50 M^{-1}), $K_{a\ [ANTS/DPX]}$ is the association constant (490 M^{-1}), $[DPX]_0$ is the initial concentration of entrapped DPX, and α is the preferential release parameter. All values of α greater than zero are indicative of graded release. If α is reduced to zero and Q_{in} does not vary with f_{out}, then the leakage represents an all-or-none mechanism. Graded release is an indication of membrane disruption, thinning or transient pore formation, while all-or-none release occurs through pore formation or vesicle lysis [65,66].

All fluorescence studies have been performed using a Molecular Devices SpectraMax M5 in which the ANTS dye is excited at 360 nm and detected at 520 nm. All runs (n = 26) have been performed with a lipid concentration of 100 μM and corrected for background fluorescence. Loaded vesicles in 0.1% TWEEN-20 is used as a control because it gives the maximum fluorescence in the absence of quenching and is used to calculate all Q values ($Q_{[DPX]} = F_{[DPX]}/F_{max}$). Incremental additions of 1 M DPX to the lysed vesicles at 1 μL intervals have been performed to prevent large volume changes, and provides the fluorescence values needed to calculate Q_{out}. The same procedure in buffer with NA-CATH provides the fluorescence values to calculate Q_{total}. A plot of Q_{total} vs. Q_{out} has been obtained for different peptide concentrations and is fitted to a line equation where the slope was f_{out}, and $b = Q_{in}(1 - f_{out})$. To account for incomplete entrapment, the Q_{total} has been measured in the absence of peptide, and the observed f_{out} is corrected with the following equation: $f_{cor} = (f_{obs} - f_o)/(1 - f_o)$. The Q_{in} vs. f_{out} (f_{cor}) correlation in which the $[DPX]_0$ and α values are allowed to vary, is fitted to Eq. (1) using the Curve Fit Toolbox in Matlab. Additionally, NA-CATH cooperativity is explored using a Hill plot (f_{out} vs. [NA-CATH]). Again, fitting to the Hill equation ($f_{out} = [P]^n/(K_{50}^n + [P]^n)$), where [P] is the concentration of the peptide (NA-CATH), n is the Hill number, and K_{50} is the peptide concentration required for half-maximum leakage using the Curve Fit Toolbox in Matlab determines if NA-CATH exhibits any positive cooperativity.

3. Results and discussion

The NA-CATH peptide is comprised of 34-amino acids and is derived from Chinese cobra venom gland [44,48]. The peptide is one of the most cationic of AMPs, consisting of two arginine and 13 lysine residues within the first 26-amino acids (Fig. 1A). This region also consists of two KKFFKK sequence repeats separated by five amino acids. There is a hydrophobic residue roughly every three amino acids within this 26-amino acid region. The last 9 amino acids of the sequence are predominantly hydrophobic with two valine, an isoleucine, a proline, and two phenylalanine residues. There are seven phenylalanine residues in which three are located near the N-terminus, two within the middle of the sequence, and two at the C-terminus. Interestingly, there are no acidic amino acids within the sequence.

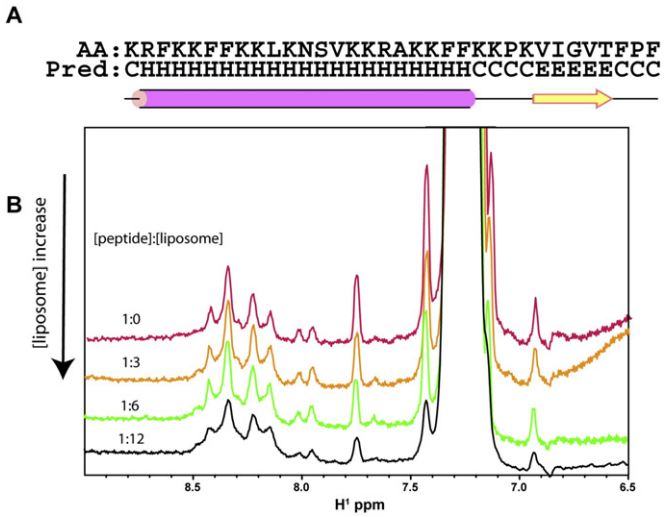

Fig. 1. NA-CATH peptide adopts a labile structure. A. The sequence of the peptide followed by summary of the secondary structure prediction. A helix is predicted for residues Arg2 to Lys23 and an extended structure is predicted for residues Val27 to Thr31. The letters under the sequence indicate the predicted secondary structure: C = coiled or unstructured region, H = helix, and E = extended structure. B. One-dimensional ^{1}H NMR spectra showing the NH and aromatic proton region of NA-CATH in aqueous solution in the absence (top spectrum) and presence of increasing concentration of 80:20 DOPC:DOPG liposomes. NA-CATH does not adopt a stable structure in aqueous solution and the similarity of the spectra indicates that most of the peptide remained unstructured in liposomes. For clarity, the spectra are colored differently. Some of the NH signals are identified and dashed lines how specific NH resonance shift with increasing concentration of liposome.

Secondary prediction by Psipred [67] of the sequence suggests the presence of an α-helix between residues Arg2 to Lys23 (Fig. 1A). Residues Val27 to Thr31 are predicted to adopt an extended structure. Previously, circular dichroism data have indicated that the peptide and the shorter ATRA-1A construct adopt a stable helical conformation in 50% TFE [19,46].

3.1. NMR studies of NA-CATH

In spite of the almost 1.5 mM peptide sample, the 1D ^{1}H spectrum of the peptide in aqueous solution shows very weak NH signals compared with the aromatic signals within the downfield (7–9 ppm) region (Fig. 1B). The 2D NOESY spectrum (100 msec mixing time) of the peptide in aqueous solution does not contain any NH-NH$_{(i,i\pm1)}$ or αH-NH$_{(i,i\pm1)}$ proton NOE characteristic of an α-helix or extended structure, respectively (data not shown). Furthermore, there are very few NH to side-chain proton–proton (^{1}H–^{1}H) correlations. Together, these observations indicate that the peptide is highly labile and does not have a stable structure and most of the NH protons are rapidly exchanging with the aqueous solution. As a result, it would not be possible to solve the structure of the peptide in aqueous solution.

Given that the peptide has been observed interacting with membranes [19,44,46,49], we next have investigated whether the peptide would adopt a stable structure in the presence of 80:20 DOPC:DOPG liposomes, which serve as a mimic of the bacterial membranes (Fig. 1B). Interestingly, the NH region of the peptide shows very little chemical shift and intensity changes. At 5–10× molar excess, there is some signal broadening indicating that the peptide maybe interacting with liposomes but not substantial broadened to conclude that the peptide is embedded in liposomes. To verify that most of the peptide may be free in solution and to identify its motion, we performed T1 and T2 relaxation measurements of the peptide in the presence and absence of liposomes. Using the signals of methyl protons, the T1 and T2 values under both conditions is estimated to be ~5.1 ± 0.4 s^{-1} and 1.9 ±

0.3 s^{-1}, respectively, confirming that the peptide is not embedded into the liposome. Furthermore, the similarity of NH signals in the absence and presence of liposomes indicate that the peptide may not adopt a stable structure in the presence of liposome.

Interestingly, upon raising the temperature of the peptide–liposome sample to 37 °C, we have observed lipids floating at the top of the solution, consistent of compromised liposomes. A control experiment with the same amount of liposomes in PBS at 37 °C, but without any peptide, does not show compromised liposomes. In fact, the liposomes are, in general, stable at 37 °C [53,57,61–63,68,69]. Similar results are observed when the peptide is titrated with 30:20:50 DOPC:DOPG:DPPC and 50:30:20 DOPC:DPPC:DPPG di-phasic vesicles that contain both the fluid and gel phases coexisting together.

Given the larger number of basic residues, we have also titrated the lipids with 50:50 DOPC:DOPG. The lines of the peptide resonances become slightly broadened with increasing concentration of liposome, but at 21 °C, the liposomes become compromised and we observe both floating and precipitated lipids.

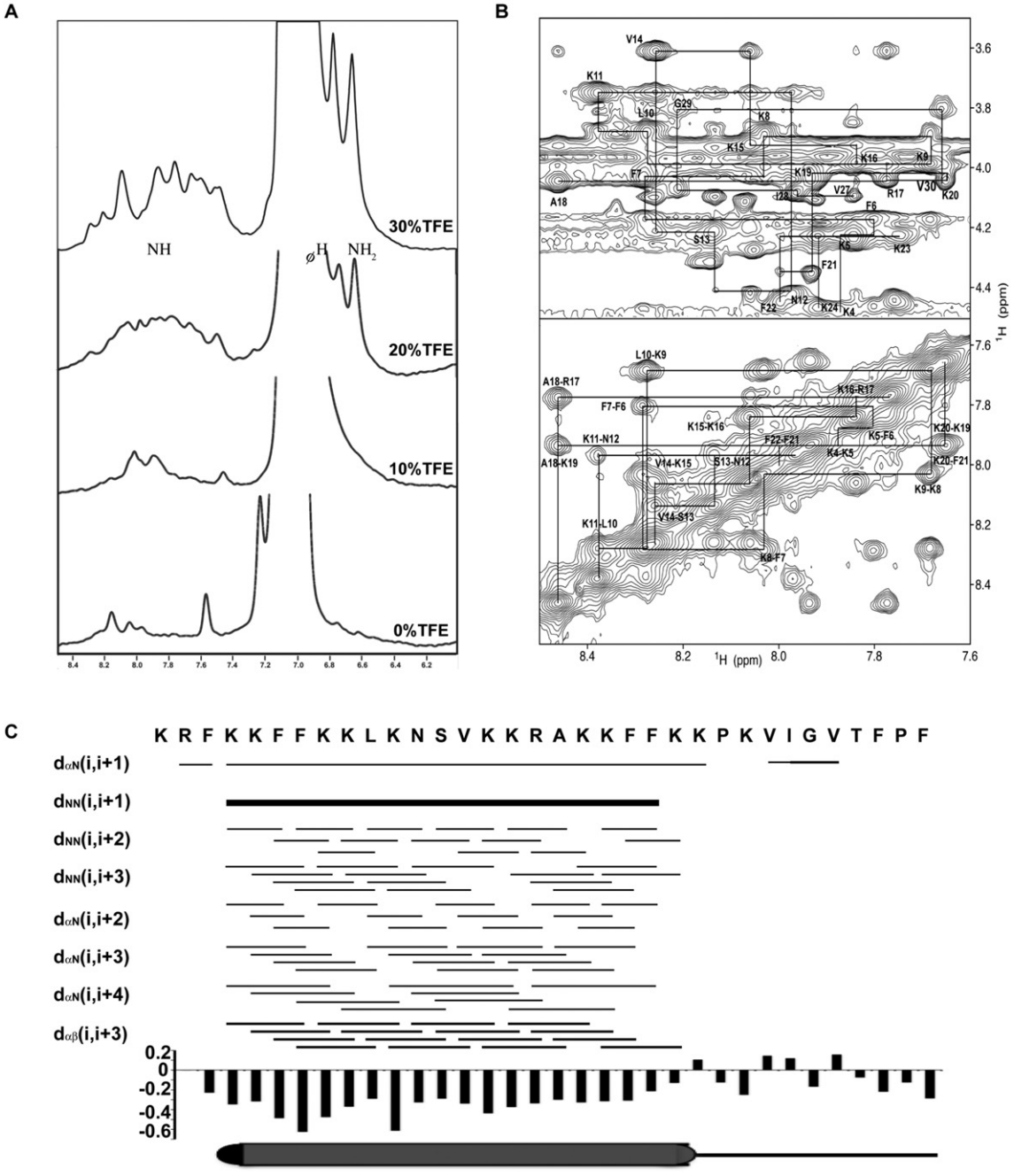

Fig. 2. NA-CATH peptide is stabilized by TFE. A. One-dimensional ^{1}H NMR spectra showing the effects of titrating of deuterated TFE on the peptide. The four spectra show the effect of 30, 20, 10, and 0% TFE (top to bottom). B. Two ^{1}H spectra showing the NH region of the peptide in TFE and liposome in the absence (top) and presence of 0.1 mM paramagnetic Mn^{2+}. The vertical scale of the spectrum of the peptide in liposome with Mn^{2+} is shown at 10 × higher since > 90% of the original NH signals intensity have decreased. Hα–NH (top) and NH–NH regions show well-resolved strong intensity ^{1}H–^{1}H NOE correlations defining the residues adopting the α-helical conformation. The intra-residue Hα resonances are labeled (top) while at the bottom, the adjacent amino acids how backbone NH protons show the NH–$NH_{(i,i+1)}$ NOEs are labeled. C. Summary of backbone sequential NOEs are shown with the thickness of the line reflecting the intensity of the NOEs. Thick lines indicate strong NOEs, while the thin lines indicate weak NOEs. At the bottom of the figure, chemical shift index of the Hα resonances for all amino acids are shown. The CSI values are based on difference in chemical shift of the observed amino acid with the corresponding amino acid in a random coil conformation. The upfield shift in Hα resonances is consistent with the extensive sequential NOEs indicating the presence of an α-helix.

3.2. NMR studies of NA-CATH in TFE

Since previous circular dichroism data have indicated that TFE stabilizes the secondary structure of the peptide [46], we have titrated deuterated TFE into the peptide. Indeed, we observe that the intensities of the NH resonances increase, with the signals becoming sharper after the first three additions of 10% TFE (Fig. 2A). There are upfield shifts of the aromatic signals (6.8–7.3 ppm) as well as aromatic ^{1}H signals becoming better resolved. No further changes of signals are observed for >30% TFE, indicating that the structure of the peptide is fully stabilized in 30% TFE. The chemical shift changes and increases in sharpness and the intensities of NH signals are considerably greater than those observed when liposome is titrated into the peptide. Furthermore, the 2D ^{1}H–^{1}H NOESY spectrum shows strong intensity NH proton to side-chain NOEs (Fig. 2B). Therefore, to characterize the structure of the peptide, we have acquired 2D NMR data of the peptide in 30% TFE.

The complete ^{1}H NMR resonance assignments are obtained based on the NH–NH$_{(i,i\pm1)}$ and Hα–NH$_{(i,i+1)}$ sequential NOE connectivities and the NH-to-side chain ^{1}H–^{1}H correlations observed in the TOCSY and COSY spectra [70]. As shown with Fig. 2B,C, there are strong intensity sequential i,i + 1 backbone NH proton NOE correlations between adjacent amino acids that allow for the connectivities of the various amino acid spin patterns. There are strong intensity sequential NH–NH$_{(i,i\pm1)}$ and weaker intensity NH–NH$_{(i,i\pm2\text{–}4)}$ NOEs consistent with an α-helix formed by residues Phe3 to Lys23 (Fig. 2C). The intermediate intensity Hα–Hβ$^1_{(i,i+3)}$H–^{1}H NOEs observed for these residues supports the presence of the α-helix. For residues Pro25–Phe34, no ^{1}H–^{1}H NOEs consistent with a secondary structure are observed. These results indicate that TFE serves to merely stabilize the structure of the peptide rather than induce helical structure since the C-terminal residues remain unstructured.

The backbone and side-chain protons for all but the N-terminal lysine residue are identified. Strong intensity Hα–Hδ$_{(i,i-1)}$ proton NOEs between the proline and the preceding amino acid indicate that the two proline residues are in the trans-conformation. The signal dispersion of the amino acid spin-systems is sufficient in the 2D NOESY and TOCSY spectra to resolve the assigned amino acids. We have been able to make backbone and side-chain atom NMR assignments for all but the first two amino acids. We are unable to assign ^{1}Hε and guanidinium protons of the arginine and the ^{1}Hε and ^{1}Hζ protons of lysine residues, which are typically the case for these long side-chains that exhibit mobility.

Chemical shift index (CSI) analysis is performed of the Hα resonances because the peptide is unlabeled (Fig. 2C). It is not feasible to acquire natural abundance ^{13}C spectrum to obtain ^{13}Cα chemical shift for CSI analysis at such low peptide concentration. Nonetheless, the Hα resonances are equally effective in identifying secondary structure elements [71,72]. The Hα atoms chemical shifts are upfield shifted by an average of 0.3 ppm for residues Phe3–Lys23, confirming the α-helix identified by backbone NH–NH$_{(i,i\pm1)}$ sequential NOEs (Fig. 2C) [72]. The Hα chemical shifts show alternating upfield and downfield shifts for the last 11 residues, consistent with random or labile structure.

3.3. Structure of NA-CATH

A total of 399 NOE-based restraints, obtained from the NOESY spectra, are used to calculate the structure of the full-length peptide (Table 1). Of these, 90 restraints are sequential, while 101 are medium range (i,i + 2–4) restraints. These restraints and structural statistics are summarized in Table 1. There are no long-range (i,i > 4) NOEs, consistent with a lack of a tertiary structure. Of the 30 structures calculated, none has NOEs and angle violations greater than 0.20 Å and 3°, respectively. There are also no vdw violations nor any deviations in bond lengths. Ten final structures are selected based on their lowest target energies and the value of their backbone atom superposition. The RMSD value for the superposition of the backbone heavy atoms for residues Phe3 to Lys23 is 0.27 ± 0.08 Å, indicating that the α-helix is well defined (Fig. 3A(I)). The helix terminates at residue Lys24, which precedes a proline residue. The relative positions for residues 1–2 and 25–34 are not defined due to the lack of NOE-based restraints caused by their structural mobility and lack of a stable structure (Fig. 3A(I,II)).

Table 1
Structure statistics for the solution structure of NA-CATH.

A. Restraint statistics	
Intra-residue NOEs	208
Sequential NOEs (|i − j| = 1)	90
Medium range NOEs (2 ≤ |i − j| ≤ 4)	101
Long range NOEs (|i − j| > 4)	0
Total NOE restraints	399
Dihedral angle restraints	0
Total restraints	399
B. Ensemble statistics analysis	
	RMSD values (Å)
Backbone heavy atoms (3–22)	0.27 ± 0.08
All heavy atoms (3–22)	0.92 ± 0.1
C. Statistics from procheck	(Ramachandran plot)
Residues in most favored regions (%)	81.4
Residues in additional allowed regions (%)	15.1
Residues in generously allowed regions (%)	3.1
Residues in disallowed regions (%)	0.3

The RMSD value for the superposition of all heavy atoms for residues Phe3 to Lys23 is 0.92 ± 0.1 Å. This slightly high RMSD value is largely due to undefined positions of the lysine and arginine side-chain Cε, Cζ, and NH$_2$ atoms, which are inherently mobile. Analyses of the 10 structures using Procheck [73] reveal that 81 % of amino acids have their dihedral angles within the most-favored region of the Ramachandran plot (Table 1), while 15% are in the additionally allowed region. For the residues within the α-helix, 95% is in the most-favored region, while 5% is in the additionally allowed region, indicating that the structure is well defined. Only one residue (Arg2) is observed in the unfavorable region. This residue is not defined in the structure calculations by any NOE-based restraint.

A depiction of the structure from the side and helical region as a helical wheel and the corresponding top-view of the α-helix (Fig. 3A(II), B(I, II)) shows the basic residues encompassing more than half of the surface of the helix. In the middle of the basic surface, a glutamine residue (Gln12) separates the two KKFFKK sequence repeats. On the opposite surface, hydrophobic residues, Phe-3, 6, 7, 21, and 22, line more of the outer ridges on the helix (Fig. 3A(I)). The electrostatic map of the helix shows two distinct surfaces, one dominated by basic residues and the other by hydrophobic residues (Fig. 3A(I,II)).

3.4. Probing the interaction of NA-CATH and liposome by NMR

As noted, the majority of the peptide in aqueous solution does not adopt a stable helical structure as it does in the presence of TFE. To understand how the full-length NA-CATH helical peptide may interact membranes, we probe the interaction of the peptide in PBS buffer and 30% TFE with liposomes (80:20 DOPC:DOPG). For these studies, we use higher concentrations of liposome (~mM range) than are typically used by the fluorescence requenching experiments because the concentration of the peptide is higher and typically such binding studies require at least 10× greater titrants, especially if the interaction is weak. The higher concentrations of peptides and liposomes are also required for detections by NMR spectroscopy.

Using 1D ^{1}H NMR spectroscopy, we have followed chemical shift changes of the peptide with increasing concentrations of liposome. Fig. 4A reveals that most of the NH proton resonances show small chemical shift changes. The NH protons of Phe3, Phe6, and Phe34 show downfield shifts with each titration point. The NH signals for Ala18, Val14, and Val30 show upfield shifts. The overlapping signals of the

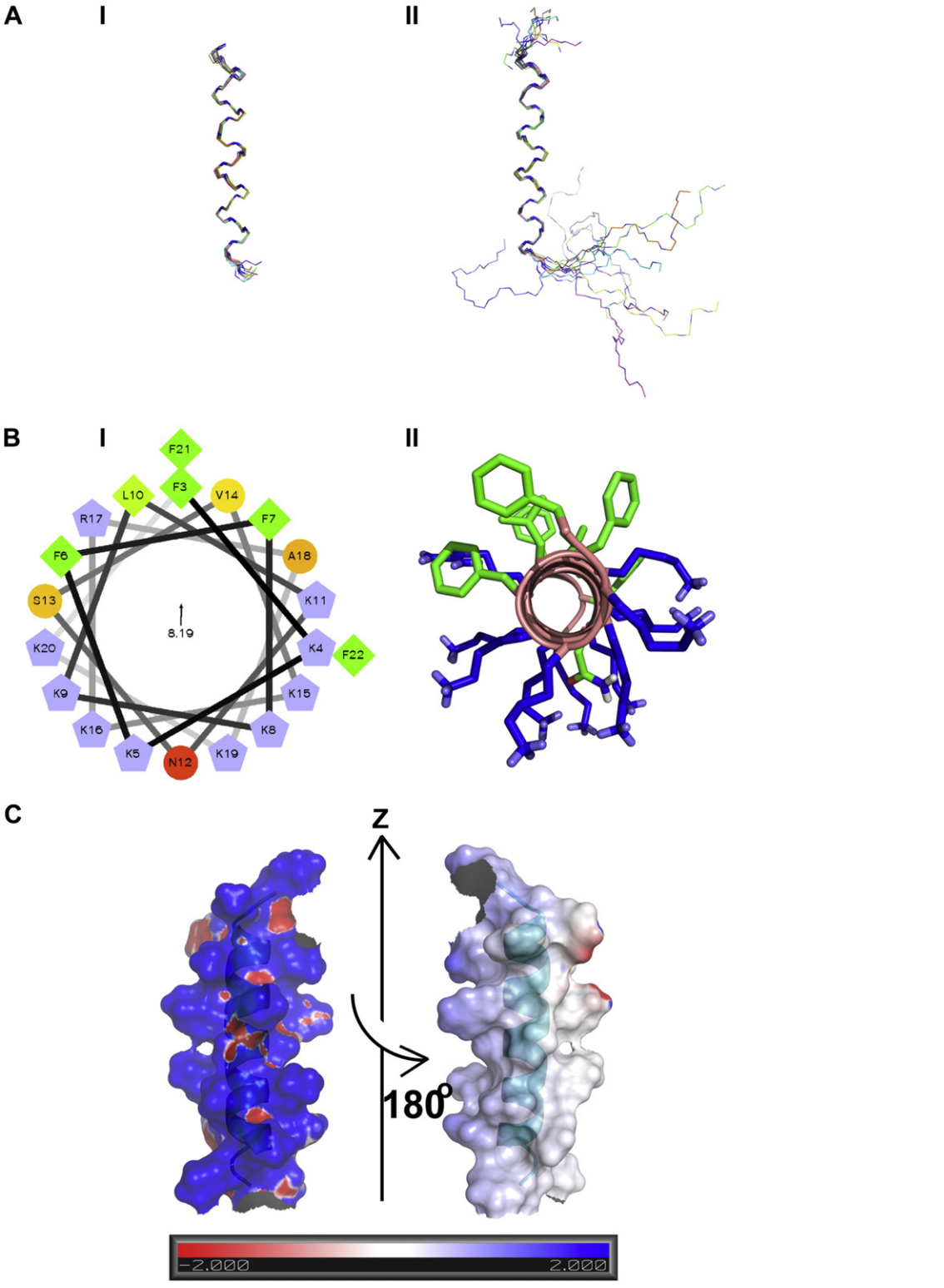

Fig. 3. Structure of NA-CATH. A. Superposition of the backbone heavy atoms of residues Phe3 to Lys24 of 10 calculated structures. (I)Shown are backbone atoms only for residues in the helical region, (II) the same superposition but the positions for residues 1–2 and 25 to 35, which are not well-defined, are reflected by their random conformations. B. Helical wheel showing position of the amino acids and the top-down view (N to C) of the calculated structure showing the position of the side-chain residues. The orientation of the helix corresponds with the helical wheel. C. Two orientations of the helix showing the electrostatic surface; on the right, the surface is made transparent to illustrate the position of the helix. The scale depicts scale from blue (basic residue) to red (acidic acid, electronegative). Blue color represents positive charged residues and the red color, here, indicates the backbone oxygen atoms. There are no negatively charged amino acids. The hydrophobic surface has a gray or whitish hue.

aromatic side-chain $^{1}H\delta/\varepsilon$ protons preclude analysis of the interaction of specific aromatic residues with the liposome but the observed signal broadening indicate that the aromatic residues are more involved with interacting with the liposome. We posit that the C-terminal tail of peptide becomes less mobile in the presence of the liposome, possibly with interacting with the liposome.

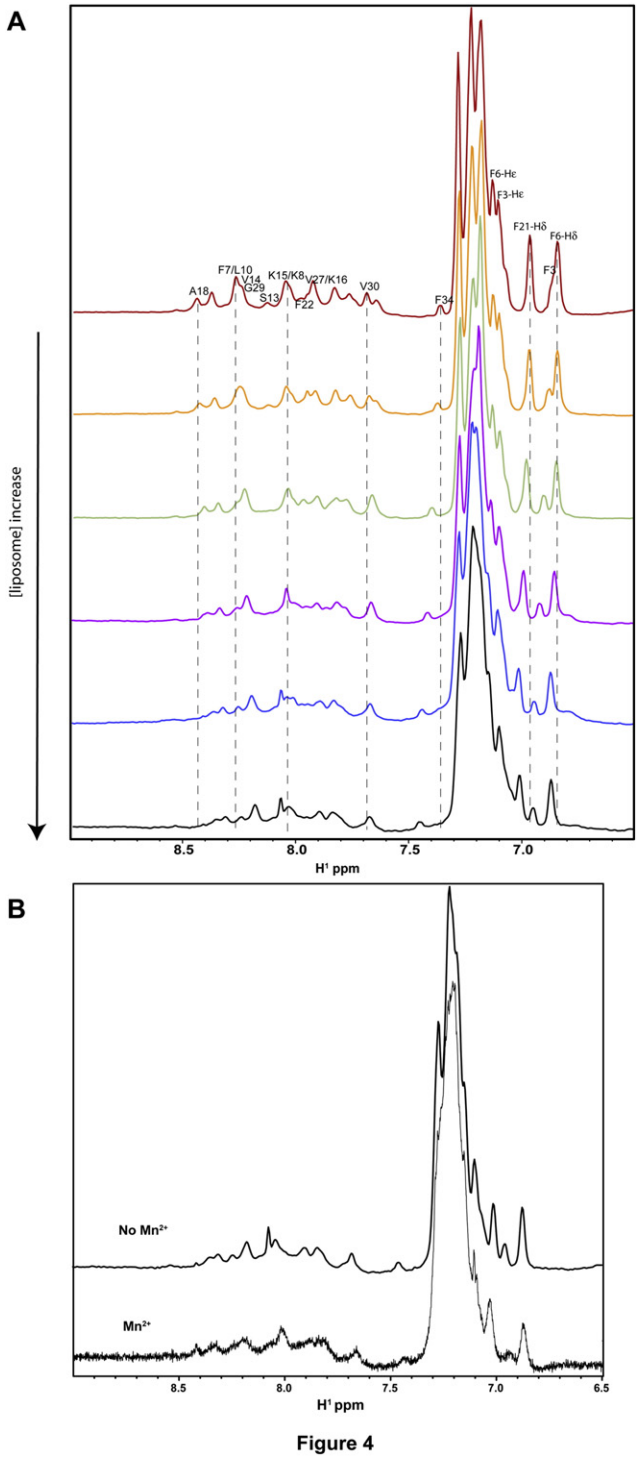

Figure 4

Fig. 4. NMR studies of the peptide–liposome interaction. A. A series of 1D ^{1}H spectra of the peptide acquired with increasing concentration of liposomes are aligned. For clarity, the spectra are colored differently. Some of the NH signals are identified and dashed lines how specific NH resonance shift with increasing concentration of liposome. B. Two spectra showing the NH region of the peptide in TFE and liposome in the absence (top) and presence of 0.1 mM paramagnetic Mn^{2+}. The spectrum of the peptide in liposome is also shown at 10× lower level since >90% of the original NH signals have been broadened.

We anticipate that if the peptide were binding strongly with the surface of the liposome or were buried within the membrane, the line-width of the peptide ^{1}H signals would be substantially broadened due to increased anisotropy. The overall line-widths of the ^{1}H resonances of the peptide remain relatively narrow and are comparable to the peptide in TFE.

To further investigate the interaction of the peptide and liposome, we have titrated paramagnetic $MnCl_2$ into the final peptide–liposome mixture (Fig. 4B). We postulate that if the peptide were embedded in the liposome the peptide signals would be protected from the paramagnetic effects of the manganese in solution [74]. After the first addition (0.1 mM $MnCl_2$), we estimate that >90% of the peptide ^{1}H signals disappear (Fig. 4B) indicating that most of the peptide is in solution. The remaining very weak ^{1}H signals suggest that a small percentage of the peptide may be embedded in the lipid bilayer to be protected from the paramagnetic effect of the manganese.

3.5. Fluorescence requenching experiments

In our recent study of NA-CATH and the shorter ATRA-1A, both peptides exhibit membrane destructive behaviors: lysing, membrane rearrangement, and content leakage [19]. However, it is unclear how NA-CATH, with such cationic content, exerts its effect on membranes. To probe a possible mechanism of action of the NA-CATH peptide with lipid bilayers, we have performed fluorescence requenching assays.

As noted, Ladokhin et al. [65] have developed a requenching protocol to differentiate between pore formation (all-or-none) and membrane disruption (graded release), and this method has been widely used by others to investigate how antimicrobial peptides initiate leakage [21,22,29,35,42]. Depending on the mechanism of leakage, the signal inside the vesicles will change as well, and it is this interior quenching (Q_{in}) that allows for the differentiation of the two. For stable pore formation, the contents inside each lysed vesicle would be released entirely (all-or-none). Any observed interior quenching (Q_{in}) will be from unlysed and unaffected vesicles. Therefore, interior quenching will remain constant with increasing fractions of leakage, and the Q_{in} vs. f_{out} plot will be a flat line, consistent with observations made by Gregory et al. for the pore-forming peptide cecropinA [22](Fig. S4). In the case of membrane permeabilization, ANTS and DPX are expected to diffuse across the membrane (graded release) and the interior concentrations will change with time. The mechanisms of permeabilization could be through membrane thinning, other membrane defects, or transient pores [29]. In this case, Q_{in} will increase as a function of ANTS and DPX leakage, and their separation and concentration will decrease. These events will increase fluorescence and will result in an upward sloping curve when Q_{in} is plotted against f_{out}, as was seen for the RTX toxins — CyaA and HiYa [21], rabbit neutrophil defensins [42], bacterial δ-lysin [41], and the cell penetrating peptide transportan 10 [35] (see Fig. S5).

In order to calculate the interior quenching (Q_{in}), we must determine the outside fluorescence and quenching in detergent (F_{out} and Q_{out}) and total fluorescence and quenching in buffer (F_{tot} and Q_{tot}). In Fig. 5A, the data show Q_{tot} measured as a function of DPX concentration at different peptide concentrations. The different curves correspond to different lipid to peptide ratios in which the top line corresponds to the most peptide present. The values of Q_{tot} increase as the concentration of peptide increases, and it corresponds to greater leakage as a function of peptide concentration.

The Q_{in} value, which is quenching within the vesicle, is then determined by plotting Q_{tot} as a function of Q_{out} (Fig. 5B). Each data series is fitted to the linear equation, $Q_{tot} = Q_{out}f_{out} + Q_{in}(1 - f_{out})$ (seeAppendix A for the full derivation) revealing a linear correlation between Q_{tot} and Q_{out}, and the values of Q_{in} and f_{out} for each lipid-to-peptide ratio. The increasing slopes of the lines (red to black lines) confirm greater leakage as a function of peptide concentration. Therefore, as the concentration of NA-CATH increases, the fraction of leakage, or f_{out} increases (Fig. 5C). The plot in Fig. 5C shows a hyperbolic relationship that fits well to the Hill equation (goodness-of-fit of 0.925), with a Hill coefficient of $n = 0.728 \pm 0.062$. This indicates that NA-CATH peptides do not form dimer or oligomeric structures.

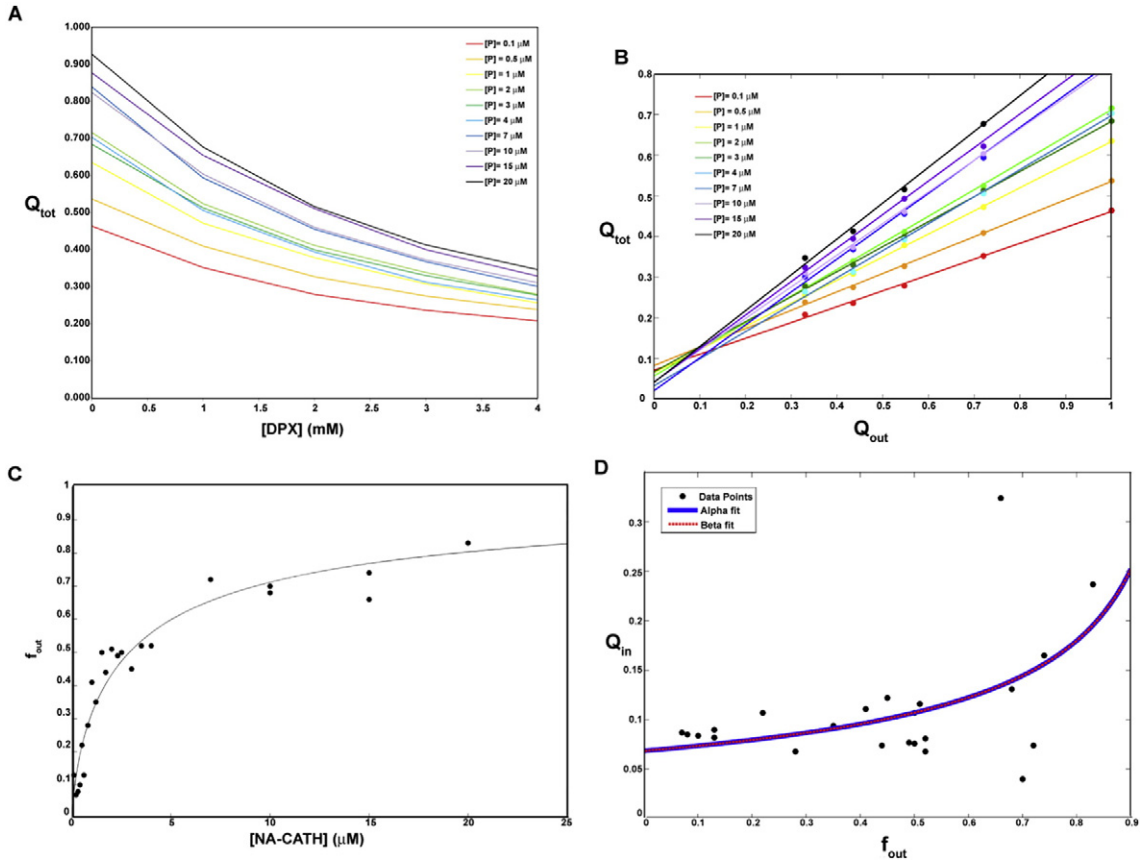

Fig. 5. Fluorescence Requenching Assay: A. Plot showing Q_{tot} vs. [DPX] (mM), where $Q_{tot} = F/F_{max}$. As DPX is titrated into the samples, fluorescence signal decreases because quenching increases. This is seen as a decrease in Q_{tot}. B. Q_{tot} vs. Q_{out}, where $Q_{tot} = F/F_{max}$ in 0.1% TWEEN-20. When Q_{tot} is plotted vs. Q_{tot} it follows the relationship $Q_{tot} = Q_{out}f_{out} + Q_{in}(1 - f_{out})$, where f_{out} is the fraction of ANTs leakage and Q_{in} is the quenching inside the vesicle. Both are specific to a particular concentration of NA-CATH. The best fit to this equation gives f_{out} as the slope, and $Q_{in}(1 - f_{out})$ as the y-intercept. C. Lysing activity v. [NA-CATH]. As NA-CATH concentration increases, so does the fraction of ANTs leakage. From the slopes of the best fits from Fig. 3C, we form the plot f_{out} vs. [NA-CATH] (μM), which shows lysing activity as a function of peptide concentration. The fit of this new curve reveals the cooperativity of NA-CATH. Using the Hill equation, we calculate its coefficient, n = 0.73 (below 1), which indicates that NA-CATH peptides do not form dimer or oligomeric structures. D. Results of the ANTS/DPX requenching assay showing the relationship of Q_{in} vs. f_{out}. By comparing the quenching inside the vesicles (Q_{in}) and the degree of fluorescence leakage (f_{out}) we see that graded release or membrane permeabilization is the predominant mechanism for NA-CATH. The fit to Eq. (1) (alpha fit, blue line) of Q_{in} vs. f_{out} data points shows that Q_{in} increases with f_{out} with $\alpha = 0.52$ and $[DPX]_0 = 0.015\ M^{-1}$. Values for $\alpha < 1$ suggest greater diffusion of ANTS across the membrane over DPX. Fitting the data to Eq. (2) (red curve) yielded an additional term (β), in which β is ratio of the fluorescence release by both mechanisms. The fit resulted in the following values: $\alpha = 0.52$, $[DPX]_0 = 0.015\ M^{-1}$, $\beta = 0.070$, $f^{grad} = 0.74$, and $f^{aon} = 0.052$. A β value <0.5 suggests the mechanism of ANTS leakage is via predominately graded, or membrane disruption.

In Fig. 5D, we compare Q_{in} and f_{out} values for different peptide concentrations. As the fraction of ANTS molecules leaks out (f_{out}), Q_{in} increases, instead of remaining constant. The clear upward trend of Q_{in} is consistent with the graded release mechanism caused by general membrane defects or transient pores, as opposed to all-or-none release through stable pores or vesicle lysis. The best fit of the data to Eq. (1) (blue curve) with parameters $K_{dDPX} = 50\ M^{-1}$ and $K_{aANTS/DPX} = 490\ M^{-1}$ provide values of $\alpha = 0.52$ and $[DPX]_0 = 0.015$ M. The preferential release parameter, α, is less than one, indicating a preferential release of ANTS over DPX. This is similar to requenching results obtained for the peptides δ-lysin and transportan 10, [35,41], where release has been shown to be graded and preferential for ANTS.

The comparison of Q_{in} and f_{out} (Fig. 5D) shows variations in data points around $f_{out} = 0.7$. To understand the cause, we performed the β analysis as described by Ladokhin et al. [65,66]. The method of analysis assumes that the leakage mechanism is complex and is a combination of graded and all-or-none release. Briefly, the coefficient, β, is defined as the preference for all-or-none release. Mathematically, it is defined as $\beta = f^{aon}/f^{grad}$, where f^{aon} is the fraction of ANTS released by the all-or-none mechanism, and f^{grad} is the fraction of ANTS released by the graded mechanism. The two fractions are related to f_{out} through the following equation: $f_{out} = f^{aon} + (1 - f^{aon})f^{grad}$. Rearrangement of these relationships and substitution into Eq. (1) gives the following new equation for Q_{in} vs. f_{out} that accounts for both mechanisms of leakage:

$$Q_{in} = \left[\left(1 + K_d[DPX]_0\left(1 - \frac{f_{out} - f^{grad}\beta}{1 - f^{grad}\beta}\right)^{\alpha}\right)\left(1 + K_a[DPX]_0\left(1 - \frac{f_{out} - f^{grad}\beta}{1 - f^{grad}\beta}\right)^{\alpha}\right)\right]^{-1}. \quad (2)$$

The best fit of this equation to our data (Fig. 5D, red curve) using the same parameters as used to fit to Eq. (1), yield values of $\alpha = 0.52$, $[DPX]_0 = 0.015$ M, $\beta = 0.070$, and $f^{grad} = 0.74$. These values match our previous calculations ($\alpha = 0.52$ and $[DPX]_0 = 0.015$ M). From these findings, the f^{aon} is calculated to be 0.052. Despite the value of f^{aon} indicating a small contribution from the all-or-none fraction, generally β values of less than 0.50 indicate a dominance of graded release [65,66]. Therefore, our β value (0.070), which is significantly less than 0.50, reveals that the mechanism of release is mostly graded caused by membrane disruption.

These fluorescent data show an increase in internal vesicle quenching consistent with changes of the DPX and ANTS concentrations within the vesicle. These observations combined with those of the NMR indicate that the leakage is due to disruption in the membrane structure. Additionally, there is no indication of positive cooperativity (Hill number, $n < 1$, see Fig. 5C) which would point towards stable pore formation [21]. With a membrane-thinning model or transient pore formation, we anticipate that the majority of the residues of the peptide will partially or completely be positioned in solution due to the loss of bilayer integrity. Membrane instability, in this case, enables bilayer rearrangement consistent with our microscopy data for both NA-CATH and ATRA-1A truncated peptide [19]. Our fluorescence assays span NA-CATH concentrations as high as 25 μM and they all indicate general structural disruption and leakage over stable pore formation behavior. However, to obtain greater detail of the mechanism of action, additional experiments such as neutron reflectometry, AFM, tagged dextrans (ranging in size from 3 kD to 10 kD) leakage assays [29,34], and other techniques [75–79], may be warranted but beyond the scope of the current studies.

In the case of the 11 amino acid ATRA-1A sequence (KRAKKFFKKLK) derived from NA-CATH, this peptide is too short to form a barrel-stave pore. Given that the peptide is shown to form an α-helix by circular dichroism in the presence of liposomes and shows similar lysing behavior with fluorescence microscopy [19], we postulate that the shorter helix disrupts the lipid bilayer with a graded disruption mechanism, similar to the full-length peptide. However, further studies are required to investigate the exact mechanism of action given that the truncated ATRA peptide lacks the long hydrophobic unstructured tail of NA-CATH, which may aid in the binding and anchoring of NA-CATH in the membrane [28]. Previous studies on other cathelicidin peptides have shown that truncated versions of these sequences retain their activity as well when the hydrophobic tail has been removed [80].

3.6. Structure and behavior of α-helical AMPs

There are numerous structures of short peptides with antibacterial activity. Although it is beyond the scope of this article to evaluate all of them, structural comparison of the NA-CATH peptide with some of these antimicrobial α-helical peptides reveals a number of differences. Within its class of α-helical AMPs, the NA-CATH helix is relatively straight (Fig. 3A(II)), in contrast to curved helical structures [81–84] and even helices separated by a helical turn[85]. For example, LL-37, a single helical cathelicidin AMP, shows considerable curvature (Fig. 6). It is not clear what contributes to the curvature in these structures. Examination of the NMR data of NA-CATH does not reveal any inter-residue side-chain proton NOEs that would indicate a curvature in the helix. The peptide structure is calculated without H-bond restraints, which can be more restrictive than those of the NOEs.

Additional differences in the structural properties of NA-CATH structure are evident when compared with other helical AMP peptides. First, the NA-CATH peptide is highly cationic with 15 lysine and arginine residues. These residues of NA-CATH are uniformly distributed along one surface of the peptide (Fig. 3A(II) & B), with most located on one surface of the helix. The hydrophobic residues are distributed along the opposite surface. The last nine C-terminal amino acids are predominantly hydrophobic and unstructured, in contrast to similar α-helical AMPs [81–85]. The few lysine and arginine residues of LL-37 (PDB: 2K6O, [84]) are located not only on the convex surface, but also on the

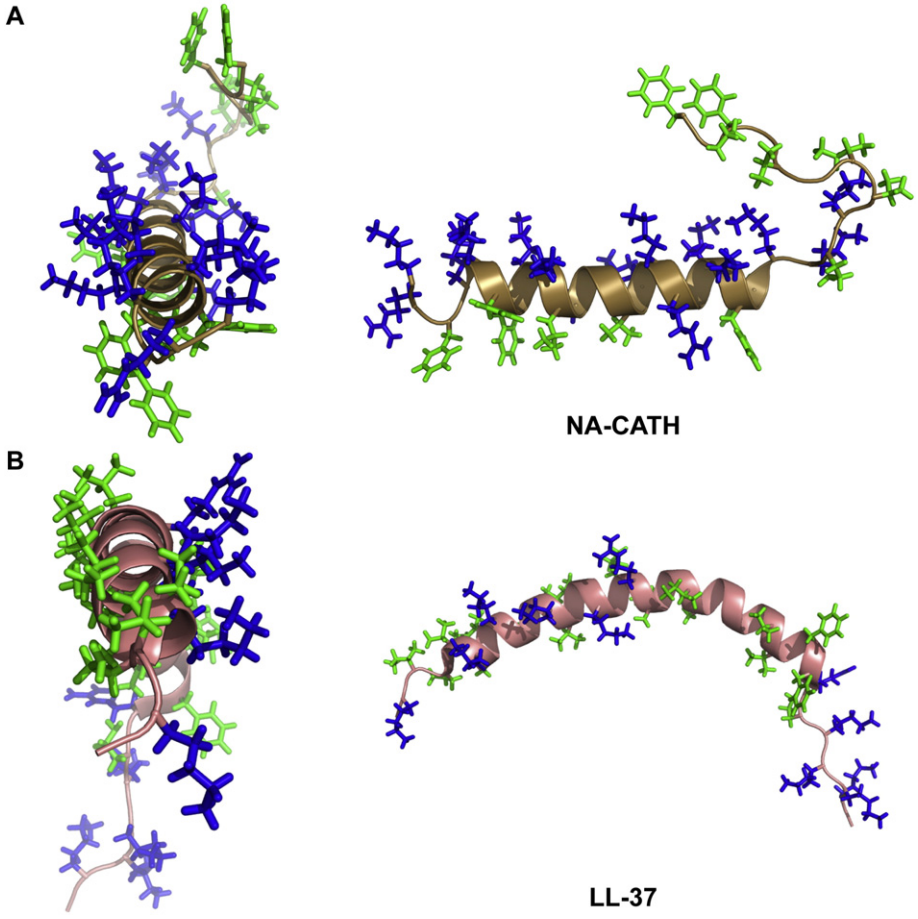

Fig. 6. Structural comparison of long α-helical antimicrobial peptides. Ribbon representation showing two orientations of the (A) NA-CATH, (B) LL-37. The arginine and lysine residues are colored blue and the hydrophobic residues are colored green.

outer edges of the helix (Fig. 6). In the LL-37 structure, a number of glutamate and asparate residues are strategically located straight along the convex surface, and this may influence the separation of the basic residues (Fig. 6). The hydrophobic residues of LL-37 are located along the concave surface.

For NA-CATH, the fluorescence data provide strong evidence of a membrane disruption mechanism of action through membrane thinning, defects, or transient pore formation, consistent with observation and previous requenching results for δ-lysin and transportan 10 [35,41]. With stable pore formation, one would expect a pattern of shielded residues, embedded in the bilayer, which is inconsistent with our NMR findings. Curved helical AMP conformations, unlike the NA-CATH NMR solution, have a propensity for pore formation [81,86] or are predicted to do so based on their structure [26,82]. According to Lad et al. [24] and Gazit et al. [87], the helix-break/bend-helix structures allow for the flexibility required to penetrate the bilayer. In contrast, long straight helical AMPs show parallel binding to the membrane leading to its disruption [20,87]. Therefore, the carpet mechanism or transient pores are likely leakage mechanisms for such AMPs. The straight helical structure of NA-CATH suggests that the membrane disruption behavior may follow this pattern.

As noted, NA-CATH has the highest positive charge of any of the peptides mentioned and this may promote interaction with the lipid headgroups and deter NA-CATH from imbedding deep in the bilayer. Such behavior fits will with the NMR peptide–liposome interaction experiments showing that significant portion of the peptide lies in solution, consistent with a compromised bilayer. Furthermore, the liposome may induce a helical structure that is too transient to be detected by NMR spectroscopy. Our previous lysing studies of the ATRA-1A peptide show similar microscopy behavior to the parent (NA-CATH) in terms of bilayer rearrangement and vesicle fusion, both indicators of bilayer instability [19]. Given the NMR and requenching data from our present investigations, the most reasonable explanation for both NA-CATH and ATRA-1A is through membrane defects or transient pore formation.

4. Conclusion

In these studies, we characterize the structure of the 34-amino acid NA-CATH peptide consisting of 15 positively charged amino acids. The region encompassing these charged residues adopts a helical confirmation. The NA-CATH structure appears to be similar to previous straight α-helical AMPs and there is strong evidence supporting a membrane disruption behavior via membrane thinning, defects, transient pores, and carpet model dissolution [20,23,32,88]. Our fluorescence and microscopy data indicate that NA-CATH functions in a similar manner. The peptide–liposome interactions probed by NMR spectroscopy reveal that a significant portion of the peptide lies in solution, consistent with a compromised bilayer. While NMR data suggest fast binding, it is possible that the disruption process occurs too rapidly to be observable by NMR spectroscopy. The fluorescence requenching studies on the other hand are able to provide insights into the mechanism of action of the peptide and complement the NMR data. We postulate from these observations, that the peptide adopts a labile structure, becoming helical when briefly bound to the liposome and lyses via membrane disruption and transient pores. However, additional studies are warranted for greater details of membrane disruption mechanism and the role the peptide structure plays in this function.

Transparency document

The Transparency document associated with this article can be found, in the online version.

Acknowledgment

This work was supported, in part, by the National Science Foundation (Award 1052520, MAM). We thank Dr. Barney Bishop (George Mason University) for many useful discussions, assistance and contributing to our NA-CATH stock.

Appendix A

In their 1997 paper, Ladokhin et al. presented the theory on differentiating between pore or graded mechanism using the ANTS/DPX dye/quencher pair and the following mathematical relationships.

$$Let \;\; F_{tot} = F_{out} + F_{in}, \tag{A1}$$

where F_{tot} is the total fluorescence signal from inside and outside the vesicles. The relationship between the quenching total, quenching inside and outside the liposomes (Q_{tot}, Q_{in} and Q_{out}) and how they affect the fluorescence signal are not simply additive. We solve for their relationship below.

Due to the presence of DPX, both F_{out} and F_{in} experience quenching, so that

$$F_{out} = Q_{out} F_{out}^{max} \;\; and \;\; F_{in} = Q_{in} F_{in}^{max} \tag{A2}$$

where, Q_{out} and Q_{in} are quenching both inside and outside the liposomes and F^{max} is the maximum possible fluorescence signal.

From combining Eqs. (A1) and (A2) we find:

$$F_{tot} = Q_{out} F_{out}^{max} + Q_{in} F_{in}^{max}. \tag{A3}$$

If we divide Eq. (A3) by F_{max} then

$$\frac{F_{tot}}{F_{max}} = Q_{out} \frac{F_{out}^{max}}{F_{max}} + Q_{in} \frac{F_{in}^{max}}{F_{max}} \tag{A4}$$

where, the total quenching is

$$Q_{tot} = \frac{F_{tot}}{F_{max}}. \tag{A5}$$

In the absence of quenching, $F_{tot} = F_{max}$, therefore $F_{tot}/F_{max} = 1$, thus allowing us to define:

$$f_{out} = \frac{F_{out}^{max}}{F_{max}}, \;\; f_{in} = \frac{F_{in}^{max}}{F_{max}}, \;\; \text{and} \;\; f_{out} + f_{in} = 1. \tag{A6}$$

By substituting Q_{tot} (A5) and the fractions of dye (A6) into Eq. (A4), we then identify the quenching relationships.

$$Q_{tot} = Q_{out} f_{out} + Q_{in} f_{in}. \tag{A7}$$

Further, if we simplify the expression using $f_{in} = 1 - f_{out}$, then

$$Q_{tot} = Q_{out} f_{out} + Q_{in}(1 - f_{out}). \tag{A8}$$

Appendix B. Supplementary data

We have included Figs. S1–S5 to provide clarity to the requenching assay data. This material is available via the Internet at http://www.sciencedirect.com. Supplementary data to this article can be found online at http://dx.doi.org/10.1016/j.bbamem.2015.07.006.

References

[1] K.A. Brogden, Antimicrobial peptides: pore formers or metabolic inhibitors in bacteria? Nat. Rev. Microbiol. 3 (2005) 238–250.

[2] J. Wiesner, A. Vilcinskas, Antimicrobial peptides: the ancient arm of the human immune system, Virulence 1 (2010) 440–464.
[3] M. Zasloff, Antimicrobial peptides of multicellular organisms, Nature 415 (2002) 389–395.
[4] K. De Smet, R. Contreras, Human antimicrobial peptides: defensins, cathelicidins and histatins, Biotechnol. Lett. 27 (2005) 1337–1347.
[5] T.B.L. Bedran, M.P.A. Mayer, D.P. Spolidorio, D. Grenier, Synergistic anti-inflammatory activity of the antimicrobial peptides human beta-defensin-3 (hBD-3) and cathelicidin (LL-37) in a three-dimensional co-culture model of gingival epithelial cells and fibroblasts, PLoS One 9 (2014).
[6] L. Wei, J.J. Yang, X.Q. He, G.X. Mo, J. Hong, X.W. Yan, D.H. Lin, R. Lai, Structure and function of a potent lipopolysaccharide-binding antimicrobial and anti-inflammatory peptide, J. Med. Chem. 56 (2013) 3546–3556.
[7] M. Pasupuleti, A. Schmidtchen, M. Malmsten, Antimicrobial peptides: key components of the innate immune system, Crit. Rev. Biotechnol. 32 (2012) 143–171.
[8] G. Wang, X. Li, Z. Wang, APD2: the updated antimicrobial peptide database and its application in peptide design, Nucleic Acids Res. 37 (2009) D933–D937.
[9] W. van't Hof, E.C.I. Veerman, E.J. Helmerhorst, A.V.N. Amerongen, Antimicrobial peptides: properties and applicability, Biol. Chem. 382 (2001) 597–619.
[10] C. Subbalakshmi, N. Sitaram, Mechanism of antimicrobial action of indolicidin, FEMS Microbiol. Lett. 160 (1998) 91–96.
[11] A. Patrzykat, C.L. Friedrich, L. Zhang, V. Mendoza, R.E.W. Hancock, Sublethal concentrations of pleurocidin-derived antimicrobial peptides inhibit macromolecular synthesis in *Escherichia coli*, Antimicrob. Agents Chemother. 46 (2002) 605–614.
[12] A. Carlsson, P. Engström, E.T. Palva, H. Bennich, Attacin, an antibacterial protein from *Hyalophora cecropia*, inhibits synthesis of outer membrane proteins in *Escherichia coli* by interfering with omp gene transcription, Infect. Immun. 59 (1991) 3040–3045.
[13] W. Brumfitt, M.R.J. Salton, J.M.T. Hamilton-Miller, Nisin, alone and combined with peptidoglycan-modulating antibiotics: activity against methicillin-resistant *Staphylococcus aureus* and vancomycin-resistant enterococci, J. Antimicrob. Chemother. 50 (2002) 731–734.
[14] G. Kragol, S. Lovas, G. Varadi, B.A. Condie, R. Hoffmann, L. Otvos, The antibacterial peptide pyrrhocoricin inhibits the ATPase actions of DnaK and prevents chaperone-assisted protein folding, Biochemistry 40 (2001) 3016–3026.
[15] L. Zhang, A. Rozek, R.E.W. Hancock, Interaction of cationic antimicrobial peptides with model membranes, J. Biol. Chem. 276 (2001) 35714–35722.
[16] A. Tossi, L. Sandri, A. Giangaspero, Amphipathic, alpha-helical antimicrobial peptides, Pept. Sci. 55 (2000) 4–30.
[17] R.M. Epand, H.J. Vogel, Diversity of antimicrobial peptides and their mechanisms of action, Biochim. Biophys. Acta Biomembr. 1462 (1999) 11–28.
[18] W.C. Wimley, Describing the mechanism of antimicrobial peptide action with the interfacial activity model, ACS Chem. Biol. 5 (2010) 905–917.
[19] M. Juba, D. Porter, S. Dean, S. Gillmor, B. Bishop, Characterization and performance of short cationic antimicrobial peptide isomers, Pept. Sci. 100 (2013) 387–401.
[20] S.S. Efimova, L.V. Schagina, O.S. Ostroumova, Channel-forming activity of cecropins in lipid bilayers: effect of agents modifying the membrane dipole potential, Langmuir 30 (2014) 7884–7892.
[21] R. Fišer, I. Konopásek, Different modes of membrane permeabilization by two RTX toxins: HlyA from *Escherichia coli* and CyaA from *Bordetella pertussis*, Biochim. Biophys. Acta Biomembr. 1788 (2009) 1249–1254.
[22] S.M. Gregory, A. Cavenaugh, V. Journigan, A. Pokorny, P.F.F. Almeida, A quantitative model for the all-or-none permeabilization of phospholipid vesicles by the antimicrobial peptide cecropin A, Biophys. J. 94 (2008) 1667–1680.
[23] A.J. Krauson, J. He, W.C. Wimley, Determining the mechanism of membrane permeabilizing peptides: identification of potent, equilibrium pore-formers, Biochim. Biophys. Acta Biomembr. 1818 (2012) 1625–1632.
[24] M.D. Lad, F. Birembaut, L.A. Clifton, R.A. Frazier, J.R.P. Webster, R.J. Green, Antimicrobial peptide–lipid binding interactions and binding selectivity, Biophys. J. 92 (2007) 3575–3586.
[25] A.S. Ladokhin, M.E. Selsted, S.H. White, Bilayer interactions of indolicidin, a small antimicrobial peptide rich in tryptophan, proline, and basic amino acids, Biophys. J. 72 (1997) 794–805.
[26] C. Landon, H. Meudal, N. Boulanger, P. Bulet, F. Vovelle, Solution structures of stomoxyn and spinigerin, two insect antimicrobial peptides with an alpha-helical conformation, Biopolymers 81 (2006) 92–103.
[27] C.-C. Lee, Y. Sun, S. Qian, H.W. Huang, Transmembrane pores formed by human antimicrobial peptide LL-37, Biophys. J. 100 (2011) 1688–1696.
[28] L.T. Nguyen, E.F. Haney, H.J. Vogel, The expanding scope of antimicrobial peptide structures and their modes of action, Trends Biotechnol. 29 (2011) 464–472.
[29] J.M. Rausch, J.R. Marks, R. Rathinakumar, W.C. Wimley, β-Sheet Pore-forming peptides selected from a rational combinatorial library: mechanism of pore formation in lipid vesicles and activity in biological membranes, Biochemistry 46 (2007) 12124–12139.
[30] J.M. Saugar, M.J. Rodríguez-Hernández, G. Beatriz, M.E. Pachón-Ibañez, M. Fernández-Reyes, D. Andreu, J. Pachón, L. Rivas, Activity of cecropin A-melittin hybrid peptides against colistin-resistant clinical strains of *Acinetobacter baumannii*: molecular basis for the differential mechanisms of action, Antimicrob. Agents Chemother. 50 (2006) 1251–1256.
[31] V. Teixeira, M.J. Feio, M. Bastos, Role of lipids in the interaction of antimicrobial peptides with membranes, Prog. Lipid Res. 51 (2012) 149–177.
[32] S. Thennarasu, A. Tan, R. Penumatchu, C.E. Shelburne, D.L. Heyl, A. Ramamoorthy, Antimicrobial and membrane disrupting activities of a peptide derived from the human cathelicidin antimicrobial peptide LL37, Biophys. J. 98 (2010) 248–257.
[33] W. Wang, D.K. Smith, K. Moulding, H.M. Chen, The dependence of membrane permeability by the antibacterial peptide cecropin b and its analogs, CB-1 and CB-3, on liposomes of different composition, J. Biol. Chem. 273 (1998) 27438–27448.
[34] W.C. Wimley, M.E. Selsted, S.H. White, Interactions between human defensins and lipid bilayers: evidence for formation of multimeric pores, Protein Sci. 3 (1994) 1362–1373.
[35] L.E. Yandek, A. Pokorny, A. Florén, K. Knoelke, Ü. Langel, P.F.F. Almeida, Mechanism of the cell-penetrating peptide transportan 10 permeation of lipid bilayers, Biophys. J. 92 (2007) 2434–2444.
[36] Y. Shai, Mechanism of the binding, insertion and destabilization of phospholipid bilayer membranes by α-helical antimicrobial and cell non-selective membrane-lytic peptides, Biochim. Biophys. Acta Biomembr. 1462 (1999) 55–70.
[37] Y. Shai, Mode of action of membrane active antimicrobial peptides, Pept. Sci. 66 (2002) 236–248.
[38] L. Yang, T.M. Weiss, R.I. Lehrer, H.W. Huang, Crystallization of antimicrobial pores in membranes: magainin and protegrin, Biophys. J. 79 (2000) 2002–2009.
[39] K. Matsuzaki, Why and how are peptide–lipid interactions utilized for self-defense? Magainins and tachyplesins as archetypes, Biochim. Biophys. Acta Biomembr. 1462 (1999) 1–10.
[40] D. Alves, M. Olívia Pereira, Mini-review: antimicrobial peptides and enzymes as promising candidates to functionalize biomaterial surfaces, Biofouling 30 (2014) 483–499.
[41] A. Pokorny, P.F.F. Almeida, Kinetics of dye efflux and lipid flip-flop induced by δ-lysin in phosphatidylcholine vesicles and the mechanism of graded release by amphipathic, α-helical peptides, Biochemistry 43 (2004) 8846–8857.
[42] K. Hristova, M.E. Selsted, S.H. White, Interactions of monomeric rabbit neutrophil defensins with bilayers: comparison with dimeric human defensin HNP-2, Biochemistry 35 (1996) 11888–11894.
[43] A.A. Strömstedt, L. Ringstad, A. Schmidtchen, M. Malmsten, Interaction between amphiphilic peptides and phospholipid membranes, Curr. Opin. Colloid Interface Sci. 15 (2010) 467–478.
[44] F.A. de Latour, L.S. Amer, E.A. Papanstasiou, B.M. Bishop, M.L.v. Hoek, Antimicrobial activity of the Naja atra cathelicidin and related small peptides, Biochem. Biophys. Res. Commun. 396 (2010) 825–830.
[45] L.S. Amer, B.M. Bishop, M.L. van Hoek, Antimicrobial and antibiofilm activity of cathelicidins and short, synthetic peptides against *Francisella*, Biochem. Biophys. Res. Commun. 396 (2010) 246–251.
[46] S.N. Dean, B.M. Bishop, M.L. van Hoek, Natural and synthetic cathelicidin peptides with anti-microbial and anti-biofilm activity against *Staphylococcus aureus*, BMC Microbiol. 11 (2011).
[47] S.N. Dean, B.M. Bishop, M.L. van Hoek, Susceptibility of *Pseudomonas aeruginosa* biofilm to alpha-helical peptides: D-enantiomer of LL-37, Front. Microbiol. 2 (2011).
[48] H. Zhao, T.-X. Gan, X.-D. Liu, Y. Jin, W.-H. Lee, J.-H. Shen, Y. Zhang, Identification and characterization of novel reptile cathelicidins from elapid snakes, Peptides 29 (2008) 1685–1691.
[49] M.L. Juba, D.K. Porter, E.H. Williams, C.A. Rodriguez, S.M. Barksdale, B.M. Bishop, Helical cationic antimicrobial peptide length and its impact on membrane disruption, Biochim. Biophys. Acta Biomembr. 1848 (2015) 1081–1091.
[50] F. Delaglio, S. Grzesiek, G.W. Vuister, G. Zhu, J. Pfeifer, A. Bax, NMRPipe: a multidimensional spectral processing system based on UNIX pipes, J. Biomol. NMR 6 (1995) 277–293.
[51] T.D. Goddard, D.G. Kneller, SPARKY 3, in, University of California, San Francisco.
[52] P. Guntert, Automated NMR structure calculation with CYANA, Methods Mol. Biol. 278 (2004) 353–378.
[53] T.G. Anderson, H.M. McConnell, A thermodynamic model for extended complexes of cholesterol and phospholipid, Biophys. J. 83 (2002) 2039–2052.
[54] M. Edidin, Lipid microdomains in cell surface membranes, Curr. Opin. Struct. Biol. 7 (1997) 528–532.
[55] M. Edidin, Lipids on the frontier: a century of cell-membrane bilayers, Nat. Rev. Mol. Cell Biol. 4 (2003) 414–418.
[56] G.W. Feigenson, Phase boundaries and biological membranes, Annu. Rev. Biophys. Biomol. Struct. 36 (2007) 63–77.
[57] S.D. Gillmor, P.S. Weiss, Dimpled vesicles: the interplay between energetics and transient pores, J. Phys. Chem. B 112 (2008) 13629–13634.
[58] A.K. Hinderliter, P.F.F. Almeida, R.L. Biltonen, C.E. Creutz, Membrane Domain Formation by Calcium-Dependent, Lipid-Binding Proteins: Insights From the C2 Motif, Elsevier Science Bv 1998, pp. 227–235.
[59] K. Jacobson, O.G. Mouritsen, R.G.W. Anderson, Lipid rafts: at a crossroad between cell biology and physics, Nat. Rev. Mol. Cell Biol. 9 (2007) 7–14.
[60] D. Lingwood, J. Ries, P. Schwille, K. Simons, Plasma membranes are poised for activation of raft phase coalescence at physiological temerature, Proc. Natl. Acad. Sci. 105 (2008) 10005–10010.
[61] H.M. McConnell, M. Vrljic, Liquid–liquid immiscibility in membranes, Annu. Rev. Biophys. Biomol. Struct. 32 (2003) 469–492.
[62] G. van Meer, D.R. Voelker, G.W. Feigenson, Membrane lipids: where they are and how they behave, Nat. Rev. Mol. Cell Biol. 9 (2008) 112–124.
[63] M.S. Kessler, R.L. Samuel, S.D. Gillmor, Polka-dotted vesicles: lipid bilayer dynamics and cross-linking effects, Langmuir 29 (2013) 2982–2991.
[64] V. Weissig, Liposomes: Methods and Protocols, Humana Press, New York, 2010.
[65] A.S. Ladokhin, W.C. Wimley, K. Hristova, S.H. White, Mechanism of leakage of contents of membrane vesicles determined by fluorescence requenching, Methods Enzymol. 278 (1997) 474–486.
[66] A.S. Ladokhin, W.C. Wimley, S.H. White, Leakage of membrane vesicle contents: determination of mechanism using fluorescence requenching, Biophys. J. 69 (1995) 1964–1971.
[67] D.W.A. Buchan, F. Minneci, T.C.O. Nugent, K. Bryson, D.T. Jones, Scalable web services for the PSIPRED protein analysis workbench, Nucleic Acids Res. 41 (2013) W340–W348.
[68] S.L. Veatch, S.L. Keller, Miscibility phase diagrams of giant vesicles containing sphingomyelin, Phys. Rev. Lett. 94 (2005) 148101.

[69] S.L. Veatch, S.L. Keller, Seeing spots: complex phase behavior in simple membranes, Biochim. Biophys. Acta 1746 (2005) 172–185.
[70] K. Wuthrich, NMR of Proteins and Nucleic Acids, 1st ed. Wiley, Hoboken, New Jersey, U.S.A, 1986.
[71] N.H. Andersen, B. Cao, C. Chen, Peptide/protein structure analysis using the chemical shift index method: upfield alpha-CH values reveal dynamic helices and alpha L sites, Biochem. Biophys. Res. Commun. 184 (1992) 1008–1014.
[72] D.S. Wishart, B.D. Sykes, F.M. Richards, The chemical shift index: a fast and simple method for the assignment of protein secondary structure through NMR spectroscopy, Biochemistry 31 (1992) 1647–1651.
[73] R.A. Laskowski, M.W. MacArthur, D.S. Moss, J.M. Thornton, PROCHECK: a program to check the stereochemical quality of protein structures, J. Appl. Crystallogr. 26 (1993) 283–291.
[74] H. Du, M.A. Massiah, NMR studies of the C-terminus of alpha4 reveal possible mechanism of its interaction with MID1 and protein phosphatase 2A, PLoS One 6 (2011) e28877.
[75] S. Singh, G. Kasetty, A. Schmidtchen, M. Malmsten, Membrane and lipopolysaccharide interactions of C-terminal peptides from S1 peptidases, Biochim. Biophys. Acta Biomembr. 1818 (2012) 2244–2251.
[76] A. Schmidtchen, L. Ringstad, G. Kasetty, H. Mizuno, M.W. Rutland, M. Malmsten, Membrane selectivity by W-tagging of antimicrobial peptides, Biochim. Biophys. Acta Biomembr. 1808 (2011) 1081–1091.
[77] A.J. García-Sáez, S. Chiantia, J. Salgado, P. Schwille, Pore formation by a bax-derived peptide: effect on the line tension of the membrane probed by AFM, Biophys. J. 93 (2007) 103–112.
[78] L. Ringstad, E. Protopapa, B. Lindholm-Sethson, A. Schmidtchen, A. Nelson, M. Malmsten, An electrochemical study into the interaction between complement-derived peptides and DOPC mono- and bilayers, Langmuir 24 (2008) 208–216.
[79] D.I. Fernandez, A.P. Le Brun, T.C. Whitwell, M.-A. Sani, M. James, F. Separovic, The antimicrobial peptide aurein 1.2 disrupts model membranes via the carpet mechanism, Phys. Chem. Chem. Phys. 14 (2012) 15739–15751.
[80] A. Giangaspero, L. Sandri, A. Tossi, Amphipathic α helical antimicrobial peptides, Eur. J. Biochem. 268 (2001) 5589–5600.
[81] R. Anders, O. Ohlenschläger, V. Soskic, H. Wenschuh, B. Heise, L.R. Brown, The NMR solution structure of the ion channel peptaibol chrysospermin C bound to dodecylphosphocholine micelles, Eur. J. Biochem. 267 (2000) 1784–1794.
[82] H. Dai, S. Rayaprolu, Y. Gong, R. Huang, O. Prakash, H. Jiang, Solution structure, antibacterial activity, and expression profile of *Manduca sexta* moricin, J. Pept. Sci. 14 (2008) 855–863.
[83] Y. Oizumi, H. Hemmi, M. Minami, A. Asaoka, M. Yamakawa, Isolation, gene expression and solution structure of a novel moricin analogue, antibacterial peptide from a lepidopteran insect, *Spodoptera litura*, Biochim. Biophys. Acta (BBA) Proteins Proteomics 1752 (2005) 83–92.
[84] G. Wang, Structures of human host defense cathelicidin LL-37 and Its smallest antimicrobial peptide KR-12 in lipid micelles, J. Biol. Chem. 283 (2008) 32637–32643.
[85] Y.R. Bommineni, H. Dai, Y.-X. Gong, J.L. Soulages, S.C. Fernando, U. DeSilva, O. Prakash, G. Zhang, Fowlicidin-3 is an α-helical cationic host defense peptide with potent antibacterial and lipopolysaccharide-neutralizing activities, FEBS J. 274 (2007) 418–428.
[86] T.A. Balashova, Z.O. Shenkarev, A.A. Tagaev, T.V. Ovchinnikova, J. Raap, A.S. Arseniev, NMR structure of the channel-former zervamicin IIB in isotropic solvents, FEBS Lett. 466 (2000) 333–336.
[87] E. Gazit, I.R. Miller, P.C. Biggin, M.S.P. Sansom, Y. Shai, Structure and orientation of the mammalian antibacterial peptide cecropin P1 within phospholipid membranes, J. Mol. Biol. 258 (1996) 860–870.
[88] S. Arcidiacono, J.W. Soares, A.M. Meehan, P. Marek, R. Kirby, Membrane permeability and antimicrobial kinetics of cecropin P1 against *Escherichia coli*, J. Pept. Sci. 15 (2009) 398–403.